frontiers in Earth Science

ORIGINAL RESEARCH
published: 24 November 2020
doi: 10.3389/feart.2020.596283

Stress-Related Pre-Seismic Water Radon Concentration Variations in the Panjin Observation Well, China (1994–2020)

Zhihua Zhou[1], Lei Tian[1], Jing Zhao[1], Haiyan Wang[2] and Jianguang Liu[3]*

[1]Department of Earthquake Prediction, China Earthquake Networks Center, Beijing, China, [2]Liaoning Earthquake Station, Liaoning Earthquake Administration, Shenyang, China, [3]Panjin Earthquake Station of Liaoning Province, Panjin, China

Continuous observation data from a period of 26 years show that water radon concentrations in the Panjin observation well document pre-seismic anomalies prior to earthquakes of $4.8 \leq M \leq 7$ within a radius of 300 km. Among these earthquakes, two distinct groups with different water radon concentration anomalies and anomaly mechanisms are apparent. The abnormal characteristics of water radon concentrations clearly reflect the processes of stress change, while Cl^- concentration, Ca^{2+} concentration, Mg^{2+} concentration, and escaping gas flow only document part of these processes. According to Global Positioning System main strain rate fields and area strain rate fields, the change in anomalous behavior coincides with the 2011 Great Tohoku M 9.1 earthquake. This event caused the stress state of the study area, located in eastern China, to change from a relative compressive stress state to a tensile state, and may be the main reason for the change in the precursory characteristics of water radon concentrations (from increasing to decreasing prior to earthquakes). Regardless, water radon concentration in the well remains a good pre-seismic indicator for earthquakes of $M \geq 4.8$. In the near future (~50–100 years), water radon anomalies in the Panjin observation well prior to earthquakes of $M \geq 4.8$ will most likely manifest as a V-shaped concentration change. Helium and neon isotopic compositions of gas samples from the Panjin observation well show that the present relatively high levels of water radon concentrations are normal and not an earthquake precursor.

Keywords: water radon concentrations, seismic precursor, anomaly mechanisms, helium and neon isotopic compositions, Panjin observation well, regional geodynamics

OPEN ACCESS

Edited by:
Giovanni Martinelli, National Institute of Geophysics and Volcanology, Italy

Reviewed by:
Zheming Shi, China University of Geosciences, China
Carlo Sabbarese, University of Campania "Luigi Vanvitelli," Italy
Adnan Barkat, National Centre for Physics, Pakistan

****Correspondence:***
Zhihua Zhou
basalin@hotmail.com

Specialty section:
This article was submitted to Geochemistry, a section of the journal Frontiers in Earth Science

Received: *19 August 2020*
Accepted: *05 November 2020*
Published: *24 November 2020*

Citation:
Zhou Z, Tian L, Zhao J, Wang H and Liu J (2020) . Front. Earth Sci. 8:596283. doi: 10.3389/feart.2020.596283

INTRODUCTION

The half-life of radon (from here on referred to as ^{222}Rn) is short and constant (3.8 days); as a result, water radonconcentrations tend to be in equilibrium under the stable physical and chemical conditions of aquifers (Kuo et al., 2009; Ambrosino et al., 2020). Since a threefold radon increase in deep groundwater was observed before the Tashkent M 5.5 earthquake of April 26, 1966 (Woith, 2015), water radon has been widely studied as a potential seismic precursor. The stress-strain developed within Earth's crust during an earthquake changes the elastic properties of the rock, the local fracture system, and the compressibility of rock pores, causing fractures in the rock mass to open up pathways through which unusually high amounts of radon can be released (Thomas, 1988;

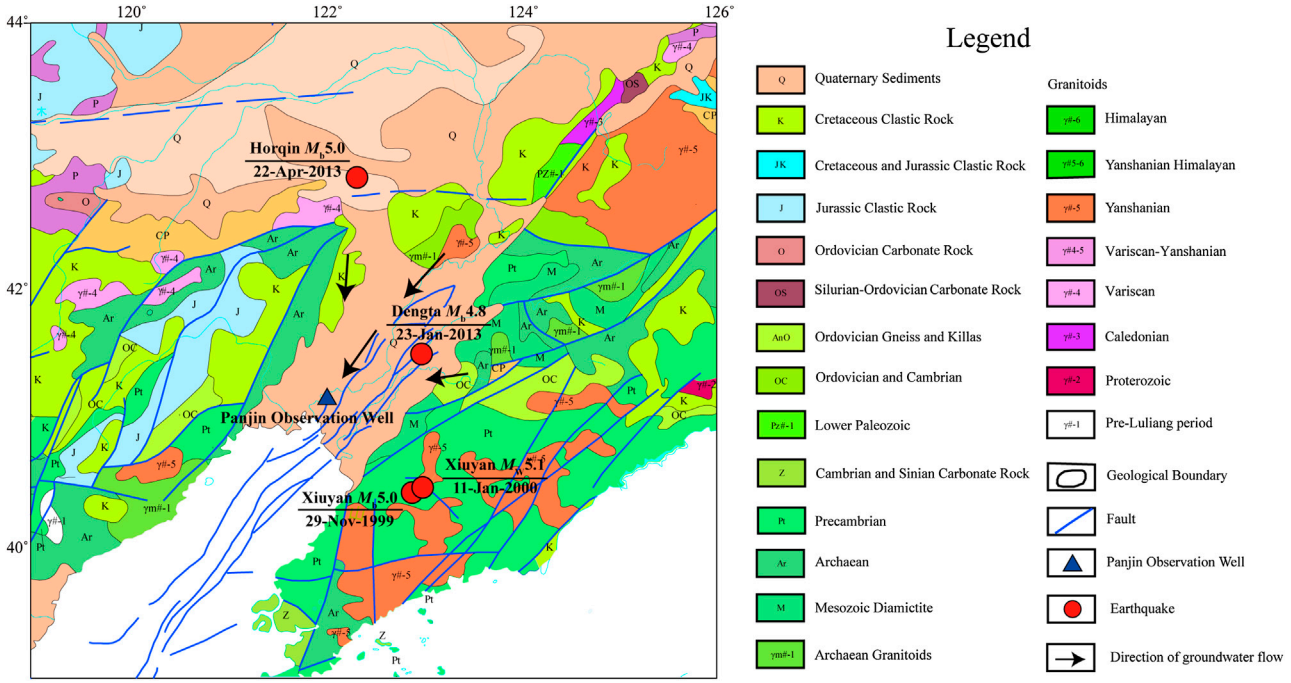

FIGURE 1 | Geographical location of Panjin observation well, Liaoning province, China. Red circles denote earthquakes of $M \geq 4.8$ within a radius of 300 km (1994–2020). The black arrows represent the groundwater flow direction of the Neogene Guantao formation.

Torgersen et al., 1990; Woith, 2015; Ambrosino et al., 2020). Most water radon observations indicate a radon increase prior to earthquakes (Hauksson, 1981; Liu et al., 1985; Igarashi and Wakita, 1990; Igarashi et al., 1995; Roeloffs, 1999; Zmazek et al., 2002; Ye et al., 2015; Kawabata et al., 2020); although, a few studies have observed decreases in water radon concentration before earthquakes (Wakita et al., 1980; Kuo et al., 2009; Namvaran and Negarestani, 2013). Regardless, it is generally believed that radon concentrations under similar geological conditions can be a sensitive indicator of strain changes in the crust preceding an earthquake and, as such, show similar precursory characteristics (Kuo et al., 2009). However, until now there have been no reports of two opposite precursory characteristics and mechanisms on one long-term continuous observation curve.

Earthquake precursors are complex processes. Time series of radon concentrations are affected by both exogenous and endogenous factors and show complex dynamics, including periodic and aperiodic oscillations on different time scales (Yan, 2018). The exogenous factors of radon concentration are common in dissolution and exchange, which are easily affected by rainfall and atmospheric pressure. Many studies have attempted to weaken the influence of exogenous factors through calculated statistical uncertainties (Asher-Bolinder et al., 1993; Heinicke et al., 2010), and to correlate anomalous increases/decreases in radon concentration with endogenous phenomena (Hauksson and Goddarard, 1981; Ambrosino et al., 2020), especially the influence of regional geodynamics on earthquake precursors. The consensus is that only long-term observation data can illustrate reliable radon precursory anomalies (Woith, 2015). In this study, we used 26 years of continuous water radon observation data, without the restriction of exogenous factors, to identify the characteristics and mechanisms of two opposite precursory anomalies observed before earthquakes. The relationship between radon precursory variations and regional geodynamics was analyzed to identify potential earthquake precursory characteristics.

GEOLOGICAL SETTINGS AND WELL BOREHOLE

The Liaohe depression is geologically located in a Cenozoic inland rift-type fault basin developed within the North China Craton, one of the world's oldest Archean cratons (Xu et al., 2014). It is at the northern extension of the Tan Lu fault zone, the main fault system of eastern China. Owing to fault activity, the Liaohe depression contains many depressions and uplifts. The study area experiences frequent earthquakes, including the 1975 Haicheng M_W 7.0 earthquake; there have been 31 earthquakes of M 5.0 or greater since 1800 (119–126°E, 39–44°N; http://www.csi.ac.cn/).

The Panjin observation well (122.02°E, 41.18°N) is located in the central, southern part of the Liaohe depression, within the middle of the second subsidence zone of the Neocathaysian structural system (**Figure 1**). The fault depression is divided

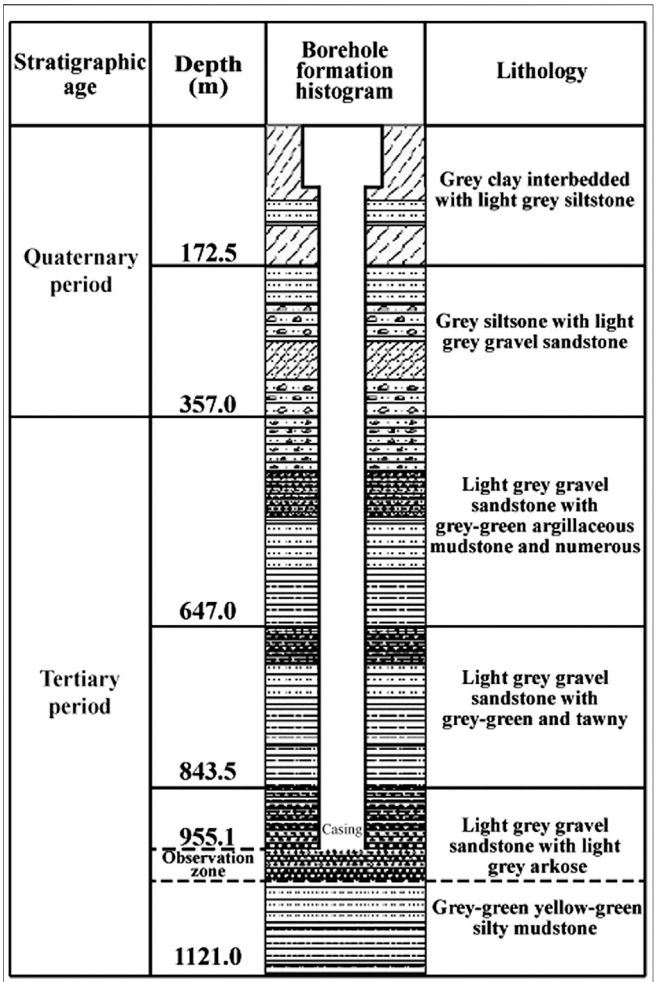

FIGURE 2 | Lithological cross-section of the Panjin observation borehole.

into six secondary structural zones by first-order major faults. The observation well is located on the Taian buried fault, a NE–SW trending normal active fault system (Lei et al., 2008). The drilling depth of the Panjin observation well is 2,892 m and the casing depth is 955.1 m. It is flowing well with confined aquifer. The base of the observed aquifer (955.1 m) is within gravel sandstone and arkose of the Neogene Guantao formation (**Figure 2**). The hydrochemical type of the observed aquifer is HCO_3-Na•Ca. The groundwater flow direction of Guantao formation is from the mountains on both sides to the middle depression, and then flows into southwest Liaodong Bay (**Figure 1**). The well is about 25 km away from the southwest coastline. In the deep aquifers of the study area, there are oil and gas exploitation layers and enriched chloride aquifers. Wang et al. (2012) showed that within the upper 360 m of depth, the shallow aquifer system has obvious vertical water circulation. Groundwater in the aquifer below 360 m constitutes an independent deep aquifer system. The vertical recharge capacity of the observation aquifer is poor; rainfall and surface water have little to no impact on the aquifer.

METHODOLOGY AND EARTHQUAKES

Monitoring Methods

Water radon concentration is measured using automatic continuous sampling once per day (1994–2020). Water is pumped out of the Panjin observation well into bubbling degassing equipment and transported into an ion chamber, where the radon concentration is measured by an ionization method using a FD-105K electrometer. When an alpha particle decays in the detector chamber, ionization of the air takes place leading to a change in the total charge on the electret. The change in the total charge results in the voltage drop over the measurement period and is used to quantify the ^{222}Rn concentration (Baskaran, 2016). The measurement precision is 0.1 Bq/L (Ye et al., 2007; Ren et al., 2012).

The Ca^{2+}, Mg^{2+}, and Cl^- concentrations and the escaping gas flow are manually sampled once a day (1994–2020). The Ca^{2+} concentration is titrated with an EDTA (ethylene diamine tetraacetic acid) standard solution at pH = 12 and the combined Ca^{2+} + Mg^{2+} concentration is titrated with an EDTA standard solution at pH = 10. The Mg^{2+} concentration is calculated using the subtraction method. The chloride concentration is obtained by titration with silver nitrate standard solution. Ion concentration precision is ~1%. Escaping gas flow is calculated by displacement water volume during the degassing process of saturated salt water; the measurement precision is 2%.

Bubbling gas samples were collected in 50-ml volume glass containers using the water displacement method; samples were taken in 2013, 2014, and 2016. He and Ne isotopes in the gas samples were measured using a MM5400 mass spectrometer. The minimum heat blanks are 1.1×10^{-14} (mol) for ^4He and 1.82×10^{-14} (mol) for ^{20}Ne, respectively. The measurements were normalized to standard atmospheric value (Ye et al., 2007; Zhou et al., 2017).

Earthquakes

Some reports show that radon anomalies can occur hundreds of kilometers from earthquake epicenters (Briestenský et al., 2014; Jilani et al., 2017; Nevinskya et al., 2018; Ambrosino et al., 2020). Jiang et al. (2019) pointed out that the distance between precursory wells and the epicenters of earthquake of $M_S < 7$ is generally less than 300 km, and that of $5 \leq M_S \leq 5.9$ is generally less than 200 km, based on a large number of earthquakes in China. Following this rules, we analyzed $5 \leq M_S < 7$ earthquakes data from 1994 to 2020 with a radius of 300km, and four eligible earthquakes were identified (http://www.csi.ac.cn/). The information they present on the USGS website is shown in **Table 1**.

Abnormal Extraction Method

We note that there are two significant changes in the measured concentration of radon in water (1999-2003 and 2011-2014) and three other less relevant changes (1994-1999, 2003-2011 and 2014-2020). Both the significant changes are found in correspondence with two groups of seismic events (**Table 1**). The occurrence of events led the background value of the

TABLE 1 | Earthquakes of $M \geq 4.8$ within 300 km of the Panjin observation well, Liaoning province (1994–2020).

Date	Location	Magnitude	Longitude (°E)	Latitude (°N)	Epicentral distance (km)
November 29, 1999	Xiuyan	M_b 5.0	122.889	40.459	108.5
January 11, 2000	Xiuyan	M_W 5.1	122.994	40.498	111.6
January 23, 2013	Dengta	M_b 4.8	122.984	41.526	89.2
April 22, 2013	Horqin	M_b 5.0	122.326	42.859	188.4

Data from https://earthquake.usgs.gov/.

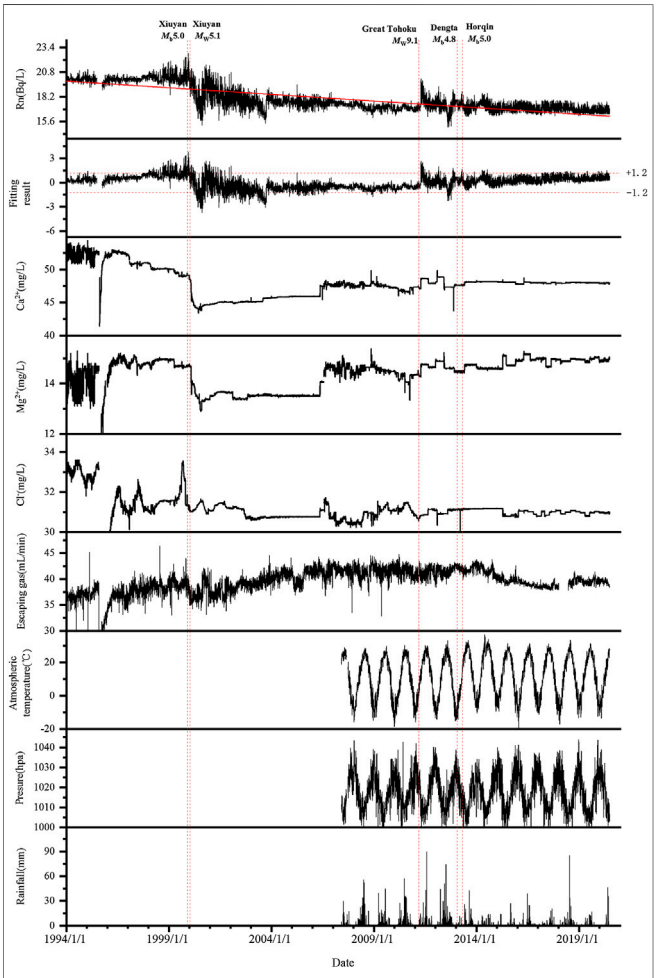

FIGURE 3 | Time series of water radon concentration, fitting result, Ca^{2+}, Mg^{2+}, and Cl^- concentrations, escaping gas flow, atmospheric temperature, pressure, and rainfall of the Panjin observation well for the period 1994–2020. The dates of earthquakes are marked by vertical red dashed lines. The red trend line is the linear fitting of the observed water radon concentration. The fitting result is calculated using the subtraction method between observed water radon concentration and the linear fitting; mean square error (MSE) is ±1.2.

observed radon concentration to decrease from 19.3 - 20.5 Bq/L (1994-1999) to 16.7-17.8 Bq/L (2003-2011), while the third observed water radon concentration change fluctuated in the range of 16.3-17.9 Bq/L (2014-2020). To compare the magnitude of these radon changes, we made a linear fit over the entire time series of the radon concentration. The result of the subtraction between the radon concentration in the measured water and that of the linear fit is shows in **Figure 3**. It was found that the amplitude of variations before the two groups of earthquakes was greater than ±1.2 of mean square error (MSE). The three other changes of water radon concentration was less than ±1.2 of MSE (**Figure 3**). The ±1.2 of MSE should be the threshold line of abnormal variation.

RESULTS

Data in the 1994–2020 times series of water radon concentrations at Panjing observation well are stable and reliable (**Figure 3**). The fitting result was calculated using the subtraction method between observed water radon concentration and the linear fitting; the mean square error (MSE) was ±1.2. Atmospheric temperature, pressure, and rainfall have been observed since June 2007 and show clear seasonal patterns. In contrast, there are no seasonal variations in the water radon concentrations or fitting results. Furthermore, August marks the rainy season, and the rainfall in August 2012 was not the historical maximum. However, the decrease in radon concentration prior to the Dengta and Horqin earthquakes was the only significant change in the time series (**Figure 3**); as such, rainfall is not responsible for the water radon changes. In summary, exogenous meteorological effects have a negligible influence on water radon in the well.

The 26 years of continuous observation data show three groups marked by significant large amplitude changes (MSE > 1.2), all of which are related to earthquakes (**Figure 3**). The first group is related to the Xiuyan M_b 5.0 and M_W 5.1 events, which occurred in 1999 and 2000, respectively. Water radon concentration increased before these earthquakes and decreased afterward. The second group is related to Great Tohoku M 9.1 earthquake of 2011. The water radon concentration increased sharply in the month following the earthquake. The third group is related to the Dengta M_b 4.8 and Horqin M_b 5.0 earthquakes in 2013. Here, there was a V-shaped progression before the earthquakes and initially low values after the earthquakes. However, the water radon concentration fluctuated for 2 years after the earthquakes, before gradually reaching a high threshold line of 1.2 times MSE.

Xiuyan M_b 5.0 and M_W 5.1 earthquakes occurred on the same fault (**Figure 1**), with a space distance of 9.9 km and a time interval of 43 days (**Table 1**). It was difficult to distinguish which earthquake caused the anomalies of observation items. Therefore,

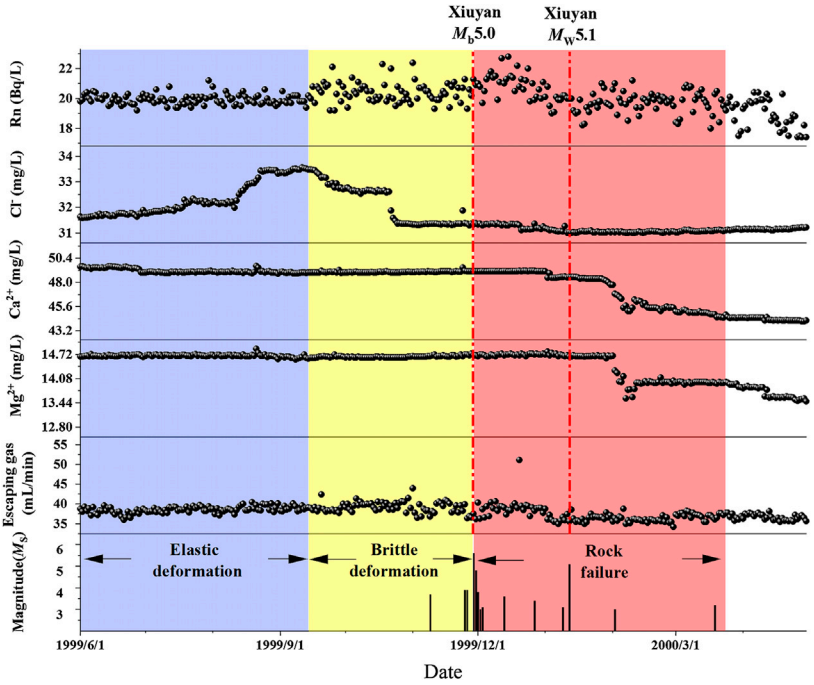

FIGURE 4 | Time series of water radon, Cl^-, Ca^{2+}, and Mg^{2+} concentrations and escaping gas flow at the Panjin observation well and their relationships to the 1999 Xiuyan M_b 5.0 and 2000 M_W 5.1 earthquakes (shown by red dashed lines). The bottom panel shows $M_S \geq 3$ foreshock and aftershock of Xiuyan earthquakes (http://www.csi.ac.cn/). Blue shading shows the elastic deformation stage; yellow shading shows the brittle deformation stage; and red shading shows the rock failure stage.

we analyzed the two earthquakes as a group. Radon concentrations around the 1999 Xiuyan earthquakes can be further split into three periods (**Figure 4**; **Table 2**). In the first stage, 80–180 days before the Xiuyan M_b 5.0 earthquake, there was no change in water radon concentration, Ca^{2+} and Mg^{2+} concentration, or escaping gas flow. The Cl^- concentration increased rapidly 110 days before the Xiuyan M_b 5.0 earthquake. The second stage was characterized by a significant increase in water radon concentration in the 80 days before the earthquake; this was accompanied by an increase in the escaping gas flow. The Cl^- concentration dropped suddenly 38 days before the earthquake. It is noteworthy that the increase in water radon concentration occurred earlier than it did for foreshocks ($M \geq 3$). In the third stage, the radon concentration decreased significantly after the Xiuyan earthquakes; the Ca^{2+} and Mg^{2+} concentrations also showed a sudden decline, but they did not change significantly before or during the earthquakes (**Table 2**).

Coincidentally, variations in the radon concentration related to the 2013 Dengta and Horqin earthquakes can also be explained by three stages; however, all occurred prior to the earthquakes (**Figure 5**; **Table 2**). In the first stage, 197 days before the Dengta earthquake, the radon concentration was stable. The Ca^{2+} and Mg^{2+} concentrations fluctuated and then dropped abruptly 237 days before the Dengta earthquake. In the second stage, 160–197 days before the earthquake, the radon concentration decreased to its lowest value (14 Bq/L). Near the third stage, the Cl^- concentration showed stepwise increases, while the radon concentration increased. The radon concentration increased to the background value 60 days before the Dengta earthquake. The change in water radon concentration had already occurred before the foreshock ($M \geq 3$). The escaping gas flow did not change significantly at any point. There was no significant change in radon concentration, Cl^- concentration, Ca^{2+} concentration, Mg^{2+} concentration, or escaping gas flow between the Dengta and Horqin earthquakes, but the radon concentration decreased significantly after the Horqin earthquake. Therefore, we analyzed the two earthquakes as a group (**Figure 5**).

DISCUSSION

Mechanism of Water Radon Anomaly in 1999

Analysis shows that pre-seismic water radon anomalies are often influenced by exogenous factors, which introduces significant uncertainty into the determination of endogenous factors (Nield and Bejan, 2006; Zafrir, 2008). Although no environmental records were recorded in 1999, significant seasonal variation can be inferred from the changes since 2007 (**Figure 3**). Seasonal changes in exogenous factors cannot explain the water radon variations before the Xiuyan M_b 5.0 and M_W 5.1 earthquakes (**Figure 3**). From the time series, the increase in radon concentrations occurred before the foreshocks of the Xiuyan earthquakes (**Figure 4**). Therefore, the anomalous changes only need to be considered in terms of the earthquake endogenous factors.

TABLE 2 | The precursory anomalies characteristics of radon and ion concentrations related to two groups of earthquakes.

Events	Processes	Time of processes	Anomaly	Rn (Bq/L)	Cl^- (mg/L)	Ca^{2+} (mg/L)	Mg^{2+} (mg/L)	Escaping gas (mL/min)
Xiuyan earthquakes	Elastic deformation	From June 1, 1999 to September 13, 1999	Start time	-	August 9, 1999	-	-	-
			Change	-	↑ 1.56	-	-	-
	Brittle deformation	From September 13, 1999 to November 29, 1999	Start time	September 13, 1999		-	-	September 20, 1999
			End time		October 21, 1999	-	-	
			Change		↓ 2.55	-	-	
	Rock failure	From November 29, 1999 to March 20, 2000	Start time		-	January 27, 2000	February 1, 2000	
			End time	December 15, 1999	-	February 12, 2000	February 12, 2000	December 15, 1999
			Change	↑ 3.00	-	↓ 6.24	↓ 1.30	↑ 17.30
Dengta and horqin earthquake	Buildup of elastic strain	From March 1, 2012 to July 10, 2012	Start time	-	-	June 1, 2012	June 1, 2012	-
			Change	-	-	↓ 1.96	↑↓ 0.68	-
	Development of cracks	From July 10, 2012 to August 13, 2012	Start time	July 10, 2012	August 8, 2012			-
			End time	August 13, 2012	August 13, 2012			-
			Change	↓ 3.2	↑ 0.31			-
	Influx of groundwater	From August 13, 2012 to April 22, 2013	Start time	August 13, 2012				-
			End time	December 18, 2012		November 29, 2012	November 29, 2012	-
			Change	↑ 4.1		↑ 0.34	↓ 0.14	-

"-" represents the normal value; The blank space represents keeping in an abnormal state.

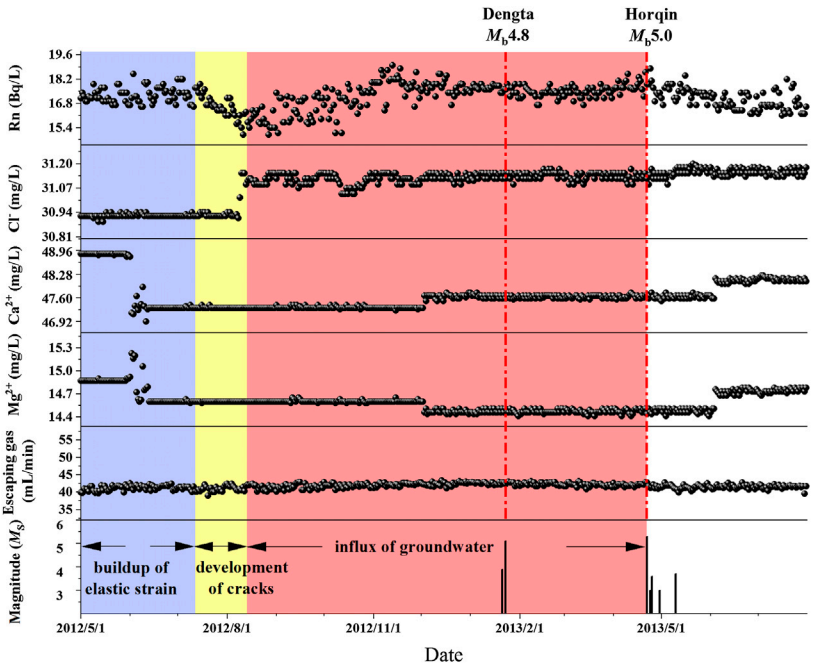

FIGURE 5 | Time series of water radon, Cl^-, Ca^{2+}, and Mg^{2+} concentrations and escaping gas flow at the Panjin observation well and their relationships to the 2013 Dengta Mb 4.8 and Horqin Mb 5.0 earthquakes (shown by red dashed lines). The bottom panel shows $M \geq 3$ foreshock and aftershock of the Dengta and Horqin earthquakes (http://www.csi.ac.cn/). Blue shading shows the buildup of elastic strain; yellow shading shows the development of cracks; and red shading shows the influx of groundwater.

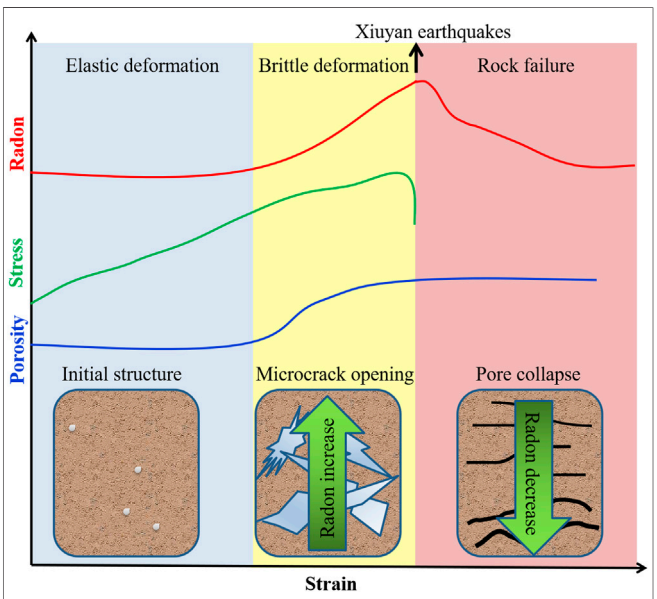

FIGURE 6 | Simplified sketch illustrating the model of radon concentration change caused by the Xiuyan earthquakes.

Gao and Zhong (2000) showed that the Xiuyan earthquakes occurred on NW trending faults under the same stress conditions (**Figure 1**). These faults are located within a new ascending NNW arched zone caused by strong crustal uplift, and the stress continued to increase before the earthquakes. The three-stage changes in radon concentration due to the earthquakes reflect three distinct processes: elastic deformation, brittle deformation, and rock failure (**Figure 4**).

Based on the pore collapse model (Schery and Gaeddert, 1982; Thomas, 1988; Toutain and Baubron, 1999), rock substrate is responsible for pore pressure changes (**Figure 6**). During the elastic deformation phase, the closure of internal pore spaces did not produce any variation in radon concentration or escaping gas flow (**Figure 4**). The rock substrate did not macroscopically fail until the end of elastic deformation, but it did cause significant irreversible microcrack damage (Mollo et al., 2018). However, this microcrack damage was not sufficient to increase radon emissions or aggravate water-rock reactions in the aquifer, as shown by the stable Ca^{2+} and Mg^{2+} concentrations. Among all the hydrochemical observations (**Figure 4**), the only one that can be proved to be in the stage of stress increase was the sudden increase of Cl^- concentration (**Figure 6**). Changing pressure in aquifer systems due to elastic compression can result in changes to Cl^- concentration (Tsunogai and Wakita, 1996). Sudden increases in Cl^- concentration can be attributed to an introduction of groundwater enriched in chloride, such as before the October 24, 1995 Wuding *M*6.5 earthquake in Yunnan (Yang, 1997) and before the September 21, 1999 Chi-Chi *M*7.3 earthquake in Taiwan (Song et al., 2005). The mixing of waters with different chemical compositions can occur quickly, and the chemical changes can also disappear rapidly (e.g., **Figure 4**; Song et al., 2006).

The brittle deformation stage conformed to the reactive surface area model (Thomas, 1988). Microcrack propagation

with increasing stress caused an increase in the surface area of the rock substrate (**Figure 6**); after which, pores ruptured and radon concentrations increased owing to the exposure of fresh rock surfaces, and escaping gas flow increased owing to the escape of trapped gas from the rock matrix (Teng, 1980; Igarashi et al., 1995; Cicerone et al., 2009). An increase in the reactive surface area should lead to more extensive water-rock interactions, and an increase in Ca^{2+} and Mg^{2+} concentrations (Claesson et al., 2007). However, there was no observed change in ion concentrations. The reason for this was that high stress can result in permeability changes within a well-aquifer system and this may break hydraulic barriers between the aquifer and other nearby small isolated reservoirs, thereby leading to mixing of chemically distinct waters (Domenico and Schwartz, 1990). However, as the volume of water added to the system is small, there would be no change in the major ions (Shi et al., 2020).

The occurrence of an earthquake marks an inflection point of stress, and this can result in radon concentration changes; that is, and increase prior to the earthquake and a decrease after (Tarakç et al., 2014). The Xiuyan earthquakes caused rock failure at a high stress level, while dike intrusions and hydrothermal fluid injections caused pervasive pore collapse at constant pressure; as a result, there was a sharp post-seismic decline in the radon concentration (Ye et al., 2015). Rock failure also caused changes in the physical and chemical properties of the observed aquifer, and this led to long-term changes in the Ca^{2+} and Mg^{2+} concentrations after earthquakes (**Figure 4**). According to the hydrochemical observations of the well in 1999 (**Figure 4**), it was found that the variations of water radon concentration could clearly show the regional geodynamic change processes, while the hydrochemical ion concentrations resulted from water-rock reactions or mixing, which led to more uncertainty.

Mechanism of the Water Radon Anomaly in 2012–2013

Decreases in radon concentration are often observed immediately after heavy rainfall (Ye et al., 2015); however, as shown in **Figure 3**, the largest rainfall in 2012 began in August, while the decline in water radon concentration began in July. In addition, August is the rainy season, and the rainfall in August 2012 was not the historical maximum, although the decrease in the radon concentration was the only significant change except for post-seismic effects. Therefore, there was no link between water radon concentration and rainfall in 2012. The Dengta M_b 4.8 earthquake was an isolated event with no foreshock and few aftershocks (Li et al., 2014). The foreshock of the Horqin M_b 5.0 earthquake occurred after the V-shaped change in the radon concentration (**Figure 5**). The stress state changes rapidly from extrusion to tension according to the aftershock information (Liu et al., 2014). It can be seen that the abnormal variation in water radon concentration in 2012 was entirely the result of endogenous factors.

Only a few other documented anomalies manifest as a decrease in pre-seismic water radon concentrations (Kuo et al., 2010; Ali Yalım et al., 2012). The process associated with this change before the Dengta earthquake can be divided into three

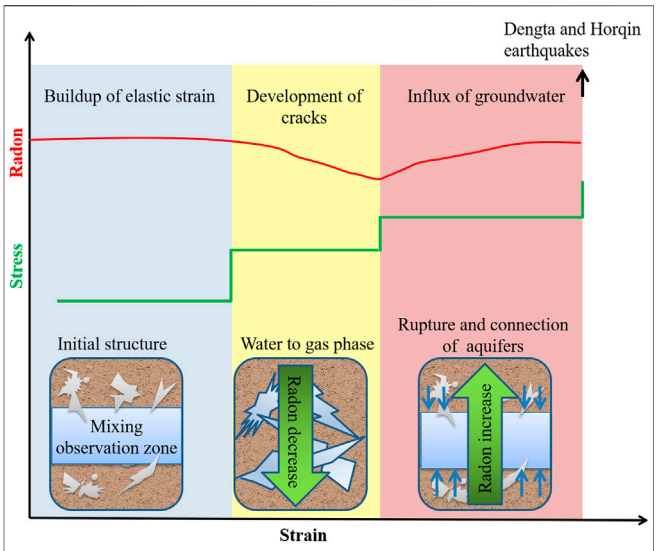

FIGURE 7 | Simplified sketch illustrating the model of radon concentration change caused by the Dengta and Horqin earthquakes.

stages (buildup of elastic strain, development of cracks, and influx of groundwater; **Figure 7**; Kuo et al., 2006), which mainly depend on the periodic changes in stress and water radon concentration. Changes in ion concentrations also reflect these stages.

During the buildup of elastic strain, the radon concentration in the groundwater was fairly stable, because the stress was relatively stable rather than gradually increasing (**Figure 7**). The stress is reflected by the sudden changes in Ca^{2+} and Mg^{2+} concentrations (**Figure 5**). According to the dilatancy-diffusion model (Scholz et al., 1973), such a change is not the result of water-rock reaction, but the result of aquifer mixing when the stress on the aquifers reaches a critical point; similar events occurred prior to the 2010 M_W 6.3 Jiasian and 2016 M_W 6.4 Meinong earthquakes (Kuo et al., 2018).

For the second stage, the stress increased suddenly, and the radon concentration decreased. Different scholars have different views on the reasons for this change. One is that the closure of cracks by small increases in compressive stress decreases radon emanation (Sultankhodzhayev et al., 1976; Fleischer and Mogrocampero, 1985), leading to reduced radon flux from crustal rocks (Einarsson et al., 2008). However, here, the escaping gas flow had no corresponding decline (**Figure 5**). The second view is that the development of new cracks in aquifer rocks can occur at a rate that is faster than the recharge of pore water (Brace et al., 1966; Scholz et al., 1973). In this scenario, dissolved radon in water is converted into a gas phase, leading to a decrease in the radon concentration of groundwater (Tsunomori and Kuo, 2010; Kuo et al., 2018). This is consistent with the decrease in radon concentration in this study, in which we also observed no change in the escaping gas flow. Additionally, because there was no pore water supply, the Ca^{2+}, Mg^{2+}, and Cl^- concentrations did not change significantly.

A further sudden increase in stress marked the third stage (**Figure 7**). The radon concentration increased owing to the

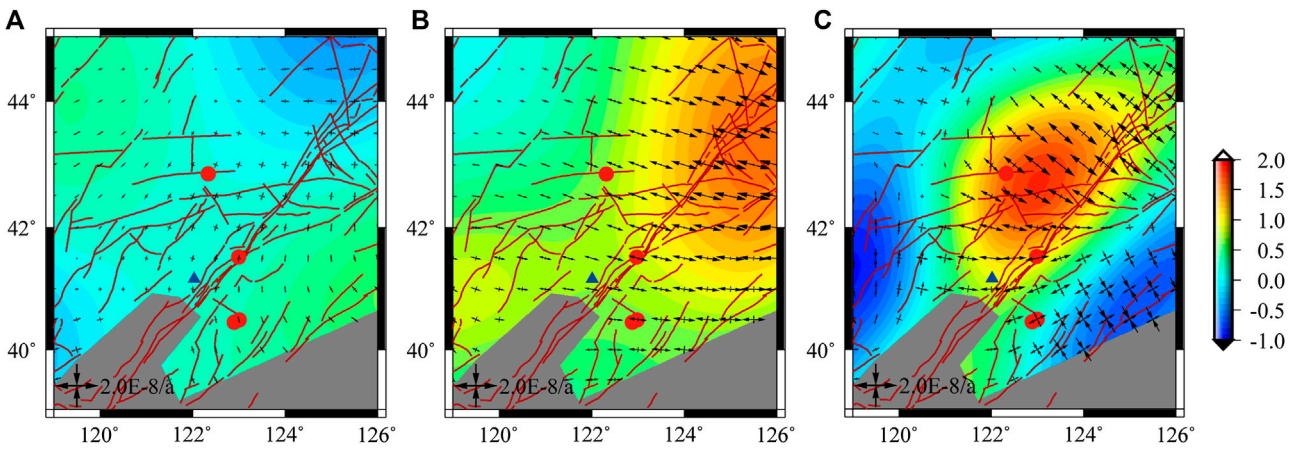

FIGURE 8 | Global Positioning System (GPS) main strain rate fields and area strain rate fields. Results for **(A)** 1999–2007, **(B)** 2011–2013, and **(C)** 2013–2016. Arrows denote the main strain rate fields and the color base map denotes the area strain rate fields. The blue triangle denotes the Panjing observation well; the red circles denote earthquake epicenters, as in **Figure 1**.

influx of groundwater, and recovered to the previous background level before the Dengta and Horqin earthquakes (**Figure 5**). The mechanism of this process was a slowing of the dilatancy rate, such that the rate of water diffusion was faster than the rate of rock dilatancy; water saturation increased and rock cracks became saturated again (Kuo et al., 2006; Kuo et al., 2010; Mollo et al., 2018). The mixing effect caused by groundwater influx, especially for groundwater enriched in chloride, can increase the chloride concentration suddenly. A continuous increase in stress results in the rupture and connection of aquifers; here, the physical and chemical properties of the aquifer changed as expected (**Figure 5**).

TABLE 3 | Chemical and isotopic compositions of gas from the Panjing observation well.

Sampling Data	$^3He/^4He$ ($\times10^{-8}$)	$^4He/^{20}Ne$	He_M[a] (%)	He_C[a] (%)	He_A[a] (%)
August 2013	165	30.88	13.62	86.38	0.00
April 2014	33	6.70	2.19	82.79	15.02
August 2016	36	13.65	2.62	90.84	6.54

[a]*He_M, He_C, and He_A denote the percentages of helium from the mantle, crust, and atmosphere, respectively.*

Explaining Two Opposing Mechanisms at Panjin Observation Well

We observed contrasting radon anomalies in the Panjin observation prior to two groups of earthquakes. Between these groups, a significant water radon anomaly occurred in 2011, a month after the Great Tohoku *M* 9.1 earthquake, for which the epicenter was 1,790 km away. We speculate that the reason for the change in water radon precursor characteristics reflects the influence of the Great Tohoku *M* 9.1 earthquake on eastern China, and particularly on regional post-seismic relaxation (Shao et al., 2015; Wang et al., 2015; Meng et al., 2019).

Endogenous factors that influence radon concentrations are primarily related to fault movement (Briestenský et al., 2014). According to Global Positioning System (GPS) main strain rate fields and area strain rate fields, there was no obvious tensile strain in the study area from 1999 to 2007 (**Figure 8A**); however, the study area experienced tensile strain after the Great Tohoku *M* 9.1 earthquake in 2011 (**Figures 8B**,C). Shao et al. (2015) also showed that the study area was in a state of compression before the Great Tohoku *M* 9.1 earthquake in 2011 and in a state of tension afterward. That is, under the condition of regional compressive strain, the stress was continuously increasing, and precursory radon anomalies in the Panjin observation well were characterized by increasing concentrations (**Figure 6**). In contrast, under a tensile strain state, the stress increased abruptly before earthquakes, and anomalies were characterized by V-shaped changes in radon concentrations (**Figure 7**). Wang et al. (2013) found that the Great Tohoku *M* 9.1 earthquake could continue to impact on the elastic relaxation of the study area for 50–100 years. Therefore, for the next ~50–100 years, precursory radon anomalies in the Panjin observation well will likely manifest as a V-shaped changes in concentration.

After the Horqin earthquake, from 2016 to 2020, the water radon concentration almost reached the upper limit of 1.2 times the MSE (**Figure 3**). To identify whether or not these high water radon concentrations represent a precursory anomaly, we carried out helium and neon isotopic compositional ($^3He/^4He$ and $^4He/^{20}Ne$) analysis of hydrothermal gas from the Panjin observation well (**Table 3**). The atmospheric $^3He/^4He$ (Ra) is 140×10^{-8}, and that of the mantle is 8 ± 1 Ra (Mamyrin and Tolstikhin, 1984). Therefore, $^3He/^4He$ is a powerful indicator for the source of volatiles entering the crust and mantle (Xu et al., 2014; Zhu et al., 2020). According to Duchkov et al. (2010), the portion of mantle helium (He_m) in the total helium of the sample (He_{meas}) can be estimated from **Equations 1**, **2**:

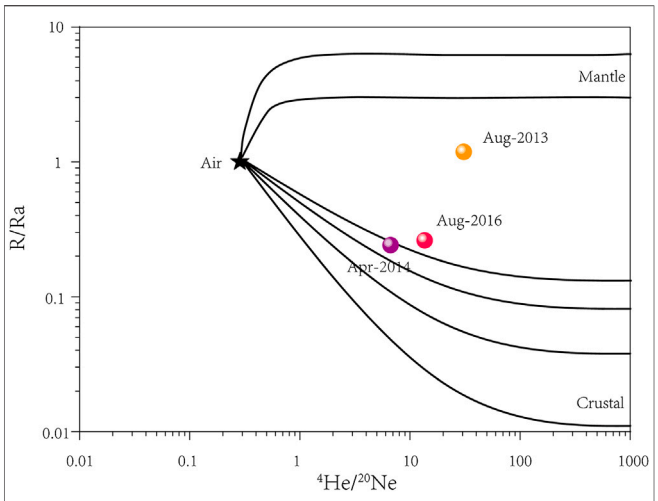

FIGURE 9 | Relationship between the R/Ra and $^4He/^{20}Ne$ ratios of hydrothermal gas in the Panjin observation well.

$$R_{cor} = \frac{R_{meas}\,(^4He/^{20}Ne)_{meas} - 42 \times 10^{-8}}{(^4He/^{20}Ne)_{meas} - 0.3} \quad (1)$$

$$\frac{He_m}{He_{meas}} \approx \frac{R_{cor} - R_c}{R_m} \approx \frac{R_{cor} - 2 \times 10^{-8}}{1,200 \times 10^{-8}}\%, \quad (2)$$

where R_{cor} is the corrected value by excluding the portion of atmospheric helium from the helium balance of the sample (Duchkov et al., 2010), R_{meas} is the $^3He/^4He$ isotopic composition of gas from the Panjing observation well, R_c is 2×10^{-8}, and R_m is $1{,}200 \times 10^{-8}$.

The atmospheric contribution to the total helium is calculated the same way, and the proportion of helium in the crust can be calculated from the difference. Calculated He_m, He_c, and He_a values are shown in **Table 3**. Mantle-derived $^3He/^4He$ represented 13.62% of the sample from mantle in 4 months after the Horqin earthquake, reflecting a post-seismic effect. Mantle-derived $^3He/^4He$ in 2014 and 2016 was ~2% (**Table 3**; **Figure 9**). The similar percentages of mantle-derived material suggest that the reaction area was under a relatively stable stress state. Furthermore, the relatively high water radon concentration in 2014–2016 occurred under a stable stress stage, and does not represent a pre-seismic anomaly.

From the analysis of GPS, $^3He/^4He$, and $^4He/^{20}Ne$, it can be concluded that the water radon concentration is relatively high owing to tensile stress in the study area. Therefore, in the future, more attention should be paid to sudden decreases in water radon concentrations, as these are more likely to be potential earthquake precursor anomalies.

CONCLUSIONS

Based on 26 years of continuous monitoring, water radon concentrations in the Panjin observation well show clear precursory responses prior to $4.8 \leq M \leq 7$ earthquakes within a distance of 300 km, suggesting that water radon in the Panjing observation well is sensitive to crustal strain within a radius of 300 km. The characteristics of the precursory response are related to the stress state, but have no relationship with the epicentral distance. Under a state of compressive stress, the observation well undergoes three stages (elastic deformation, brittle deformation, and rock failure), with water radon concentrations increasing before earthquakes (e.g., the 1999 and 2000 Xiuyan earthquakes). Under a tensile stress state, the observation well experiences three stages before earthquakes (buildup of elastic strain, development of cracks, and influx of ground water). Precursory water radon anomalies manifest as V-shaped changes in radon monitoring, such as those that occurred in 2012–2013. Changes in ion concentrations also reflected the stress change processes before both groups of earthquakes. GPS main strain rate fields and area strain rate fields suggest that the reason for the change in stress states, and as such the change in water radon precursory characteristics, is the continuing influence of the 2011 Great Tohoku M 9.1 earthquake, particularly in terms of regional post-seismic relaxation. Isotopic compositions show that the present relatively high water radon concentration is not an earthquake precursor. In the near future (~50–100 years), pre-seismic anomalies in the Panjin observation well will probably continue to manifest as V-shaped changes in water radon concentration.

DATA AVAILABILITY STATEMENT

The original contributions presented in the study are included in the article, further inquiries can be directed to the corresponding author.

AUTHOR CONTRIBUTIONS

ZZ designed the research and wrote the manuscript. LT and JZ collected data and created figures and illustrations. All authors performed the research, analyzed the results, and approved the manuscript.

FUNDING

This work was supported by the National Natural Science Foundation of China (grant number 41503114), and the China Earthquake Administration Earthquake Tracking Program (grant number 2020020302).

ACKNOWLEDGMENTS

We are grateful to Rui Yan of CENC and four reviewers for constructive comments and suggestions. We thank the First Monitoring and Application Center of China Earthquake Administration for providing the GPS velocity field datasets.

REFERENCES

Ali Yalım, H., Sandıkcıoğlu, A., Ertuğrul, O., and Yıldız, A. (2012). Determination of the relationship between radon anomalies and earthquakes in well waters on the Aksehir-Simav Fault System in Afyonkarahisar province, Turkey. *J. Environ. Radioact.* 110, 7–12. doi:10.1016/j.jenvrad.2012.01.015

Ambrosino, F., Thinová, L., Briestenskỳ, M., Guidicepietro, F., Roca, V., and Sabbarese, C. (2020). Analysis of geophysical and meteorological parameters influencing ^{222}Rn activity concentration in Mladeč caves (Czech Republic) and in soils of Phlegrean Fields caldera (Italy). *Appl. Radiat. Isot.* 160, 109140. doi:10.1016/j.apradiso.2020.109140

Asher-Bolinder, S., Owen, D. E., and Schumann, R. R. (1993). "A preliminary evaluation of environmental factors influencing day-to-day and seasonal soil-gas radon concentration," in *Field studies of radon in rocks, soils and water*. Editors L. C. S. Gundersen and R. B. Wanty (Reston, VA: U. S. Geological Survey), 23–31.

Baskaran, M. (2016). "Radon as a tracer for earthquake studies," in *Part of the Springer Geochemistry book series (SPRIGEO)*. Editor M. Baskaran, Cham: Springer, 205–228. doi:10.1007/978-3-319-21329-3

Brace, W. F., Paulding, B. W., Jr, and Scholz, C. (1966). Dilatancy in the fracture of crystalline rocks. *J. Geophys. Res.* 71, 3939–3953. doi:10.1029/jz071i016p03939

Briestenský, M., Thinová, L., Praksová, R., Stemberk, J., Rowberry, M. D., and Knejflová, Z. (2014). Radon, carbon dioxide and fault displacements in central Europe related to the Tōhoku earthquake. *Radiat. Rotect. Dosim.* 160 (1–3), 68–82. doi:10.1093/rpd/ncu090

Cicerone, R. D., Ebel, J. E., and Britton, J. (2009). A systematic compilation of earthquake precursors. *Tectonophysics* 476, 371–396. doi:10.1016/j.tecto.2009.06.008

Claesson, L., Skelton, A., Graham, C., and Mörth, C. M. (2007). The timescale and mechanisms of fault sealing and water-rock interaction after an earthquake. *Geofluids* 7 (4), 427–440. doi:10.1111/j.1468-8123.2007.00197.x

Domenico, P. A., and Schwartz, F. W. (1990). *Physical and chemical hydrogeology*. Singapore: John Wiley & Sons.

Duchkov, A. D., Rychkova, K. M., Lebedev, V. I., Kamenski, I. L., and Sokolova, L. S. (2010). Estimation of heat flow in Tuva from data on helium isotopes in thermal mineral springs. *Russ. Geol. Geophys.* 51, 209–219. doi:10.1016/j.rgg.2009.12.023

Einarsson, P., Theodórsson, P., Hjartardóttir, Á. R., and Guðjónsson, G. I. (2008). Radon changes associated with the earthquake sequence in June 2000 in the south Iceland seismic zone. *Pure Appl. Geophys.* 165, 63–74.

Fleischer, R. L., and Mogrocampero, A. (1985). Association of subsurface radon changes in Alaska and the northeastern United States with earthquakes. *Geochem. Cosmochim. Acta* 49, 1061–1071. doi:10.1016/0016-7037(85)90319-9

Gao, C. B., and Zhong, Y. Z. (2000). Geological background and seismogenic fault of the Haicheng-Xiuyan N5.6 earthquake of November 29, 1999. *Seismol. Geol.* 22 (4), 405–412 [in Chinese with English abstract]. doi:10.3969/j.issn.0253-4967.2000.04.009

Hauksson, E., and Goddard, J. G. (1981). Radon earthquake precursor studies in Iceland. *J. Geophys. Res.* 86 (B8), 7037–7054. doi:10.1029/jb086ib08p07037

Hauksson, E. (1981). Radon content of groundwater as an earthquake precursor: evaluation of worldwide data and physical basis. *J. Geophys. Res.* 86, 9397–9410. doi:10.1029/jb086ib10p09397

Heinicke, J., Italiano, F., Koch, U., Martinelli, G., and Telesca, L. (2010). Anomalous fluid emission of a deep borehole in a seismically active area of Northern Apennines (Italy). *Appl. Geochem.* 25 (4), 555–571. doi:10.1016/j.apgeochem.2010.01.012

Igarashi, G., Saeki, S., Takahata, N., Sumikawa, K., Tasaka, S., Sasaki, Y., et al. (1995). Groundwater radon anomaly before the Kobe earthquake in Japan. *Science* 269 (5220), 60–61. doi:10.1126/science.269.5220.60

Igarashi, G., and Wakita, H. (1990). Groundwater radon anomalies associated with earthquakes. *Tectonophysics* 180, 237–254. doi:10.1016/0040-1951(90)90311-u

Jiang, H. K., Yang, M. L., and Fu, H. (2019). *Earthquake cases in China (2013)*. Beijing, Seismol. Press.

Jilani, Z., Mehmood, T., Alam, A., Awais, M., and Iqbal, T. (2017). Monitoring and descriptive analysis of radon in relation to seismic activity of Northern Pakistan. *J. Environ. Radioact.* 172, 43–51. doi:10.1016/j.jenvrad.2017.03.010

Kawabata, K., Sato, T., Takahashi, H. A., Tsunomori, F., Hosono, T., Takahashi, M., et al. (2020). Changes in groundwater radon concentrations caused by the 2016 Kumamoto earthquake. *J. Hydrol.* 584, 124712. doi:10.1016/j.jhydrol.2020.124712

Kuo, M. C. T., Fan, K., Kuochen, H., and Chen, W. (2006). A Mechanism for anomalous decline in radon precursory to an earthquake. *Ground Water* 44 (5), 642–647. doi:10.1111/j.1745-6584.2006.00219.x

Kuo, T., Chen, W., and Ho, C. (2018). Anomalous decrease in groundwater radon before 2016 M_w 6.4 Meinong earthquake and its application in Taiwan. *Appl. Radiat. Isot.* 136, 68–72. doi:10.1016/j.apradiso.2018.02.015

Kuo, T., Lin, C., Fan, K., Chang, G., Lewis, C., Han, Y., et al. (2009). Radon anomalies precursory to the 2003 MW=6.8 hengkung and 2006 MW=6.1 Taitung earthquakes in Taiwan. *Radiat. Meas.* 44, 295–299. doi:10.1016/j.radmeas.2009.03.020

Kuo, T., Su, C., Chang, C., Lin, C., Cheng, W., Liang, H., et al. (2010). Application of recurrent radon precursors for forecasting large earthquakes (Mw > 6.0) near Antung, Taiwan. *Radiat. Meas.* 45, 1049–1054. doi:10.1016/j.radmeas.2010.08.009

Lei, Q. Q., Liao, X., Dong, X. Y., and Yang, S. C. (2008). Main active faults and their seismic activities in Liaoning Province. *Technol. Earthq. Disaster Prev.* 3 (2), 111–125 [in Chinese with English abstract]. doi:10.11899/zzfy20080202

Li, T. X., Chen, N., Wu, J. T., Wang, Y., Zhai, L. N., and Wang, L. (2014). A shallow study of Dengta M5.1 earthquake on January 23, 2013 in Liaoning Province. *J. Disast. Prevent. Reduc.* 30 (2), 27–30 [in Chinese with English abstract]. doi:10.13693/j.cnki.cn21-1573.2014.02.006

Liu, F., Diao, G. L., Han, X. M., Zhang, F., Jin, X. X., and Ji, B. R. (2014). Primarily discussion about the seismogenic structure of Horqin Left Back Banner *M* 5.3 earthquake on April 22, 2013. *Sesmol. Geomagn. Obs. Res.* 35 (5/6), 63–67 [in Chinese with English abstract]. doi:10.3969/j.issn.1003-3246.2014.05/06.011

Liu, K. K., Yui, T. F., Yeh, Y. H., Tsai, Y. B., and Teng, T. L. (1985). Variations of radon content in groundwaters and possible correlation with seismic activities in northern Taiwan. *Pure Appl. Geophys.* 122, 231–244. doi:10.1007/bf00874596

Mamyrin, B. A., and Tolstikhin, I. N. (1984). *Helium isotopes in nature*. Amsterdam, Netherlands: Elsevier, 273.

Meng, G. J., Su, X. N., Wu, W. W., Nikolay, S., Takahashi, H., Ohzono, M., et al. (2019). Crustal deformation of northeastern China following the 2011 Mw 9.0 Tohoku, Japan earthquake estimated from GPS observations: strain heterogeneity and seismicity. *Rem. Sens.* 11 (24), 3029. doi:10.3390/rs11243029

Mollo, S., Tuccimei, P., Soligo, M., and GalliScarlato, G. P. (2018). "Advancements in understanding the radon signal in volcanic areas: a laboratory approach based on rock physicochemical changes. Integrating disaster science and management," in *Integrating disaster science and management, global case studies in mitigation and recovery*. Editors P. Samui, D. Kim, and C. Ghosh (Amsterdam, Netherlands: Elsevier), Chap. 18, 309–328. doi:10.1016/B978-0-12-812056-9.00018-X

Namvaran, M., and Negarestani, A. (2013). Measuring the radon concentration and investigating the mechanism of decline prior an earthquake (Jooshan, SE of Iran). *J. Radioanal. Nucl. Chem.* 298, 1–8. doi:10.1007/s10967-012-2162-7

Nevinskya, I., Tsvetkovaa, T., Dogrub, M., Aksoyc, E., Inceozc, M., Baykarad, O., et al. (2018). Results of the simultaneous measurements of radon around the Black Sea for seismological applications. *J. Environ. Radioact.* 192, 48–66. doi:10.1016/j.jenvrad.2018.05.019

Nield, D. A., and Bejan, A. (2006). *Convection in porous media*. New York, NY: Springer.

Ren, H. W., Liu, Y. W., and Yang, D. Y. (2012). A preliminary study of post-seismic effects of radon following the Ms 8.0 Wenchuan earthquake. *Radiat. Meas.* 47, 82–88. doi:10.1016/j.radmeas.2011.10.005

Roeloffs, E. (1999). Radon and rock deformation. *Nature* 339, 104–105. doi:10.1038/20072

Schery, S. D., and Gaeddert, D. H. (1982). Measurements of the effect of cyclic atmospheric pressure variation on the flux of 222-Rn from the soil. *Geophys. Res. Lett.* 9, 835–838. doi:10.1029/gl009i008p00835

Scholz, C. H., Sykes, L. R., and Aggarwal, Y. P. (1973). Earthquake prediction: a physical basis. *Science* 181, 803–810. doi:10.1126/science.181.4102.803

Shao, Z. G., Zhan, W., Zhang, L. P., and Xu, J. (2015). Analysis of the far-field Co-seismic and post-seismic responses caused by the 2011 M W 9.0 Tohoku-Oki earthquake. *Pure Appl. Geophys.* 173 (2), 411–424. doi:10.1007/s00024-015-1131-9

Shi, Z. M., Zhang, H., and Wang, G. C. (2020). Groundwater trace elements change induced by M5.0 earthquake in Yunnan. *J. Hydrol.* 581, 124424. doi:10.1016/j.jhydrol.2019.124424

Song, S. R., Chen, Y. L., Liu, C. M., Ku, W. Y., Chen, H. F., Liu, Y. J., et al. (2005). Hydrochemical changes in spring waters in Taiwan: implications for evaluating sites for earthquake precursory monitoring. *Terr. Atmos. Ocean Sci.* 16, 745–762. doi:10.3319/tao.2005.16.4.745(gig)

Song, S. R., Ku, W. Y., Chen, Y. L., Liu, C. M., Chen, H. F., Chan, P. S., et al. (2006). Hydrogeochemical anomalies in the springs of the Chiayi area in west-central Taiwan as possible precusors to earthquakes. *Pure Appl. Geophys.* 163, 675–691. doi:10.1007/s00024-006-0046-x

Sultankhodzhayev, A. N., Chernov, I. G., and Zakirov, T. (1976). Hydroseismic precursors to the Gazli earthquake. *Acad. Sci. Rep. Uzbekistan* 7, 51–53.

Tarakç, M., Harman, C., Saç, M. M., and Içhedef, M. (2014). Investigation of the relationships between seismic activities and radon level in Western Turkey. *Appl. Radiat. Isot.* 83 (Part A), 12–17. doi:10.1016/j.apradiso.2013.10.008

Teng, T. L. (1980). Some recent studies on groundwater radon content as an earthquake precursor. *J. Geophys. Res.* 85 (B6), 3089–3099. doi:10.1029/jb085ib06p03089

Thomas, D. (1988). Geochemical precursors to seismic activity. *Pure Appl. Geophys.* 126, 241–265. doi:10.1007/bf00878998

Torgersen, T., Benoit, J., and Mackie, D. (1990). Controls on groundwater Rn-222 concentrations in fractured rock. *Geophys. Res. Lett.* 17, 845–848. doi:10.1029/gl017i006p00845

Toutain, J. P., and Baubron, J. C. (1999). Gas geochemistry and seismotectonics: a review. *Tectonophysics* 304 (1–2), 1–27. doi:10.1016/s0040-1951(98)00295-9

Tsunogai, U., and Wakita, H. (1996). Anomalous changes in groundwater chemistry—possible precursors of the 1995 Hyogo-ken Nanbu earthquake, Japan. *J. Phys. Earth* 44, 381–390. doi:10.4294/jpe1952.44.381

Tsunomori, F., and Kuo, T. (2010). A mechanism for radon decline prior to the 1978 Izu-Oshima-Kinkai earthquake in Japan. *Radiat. Meas.* 45 (1), 139–142. doi:10.1016/j.radmeas.2009.08.003

Wakita, H., Nakamura, Y., Notsu, K., Noguchi, M., and Asada, T. (1980). Radon anomaly: a possible precursor of the 1978 Izu-Oshima-kinkai earthquake. *Science* 207, 882–883. doi:10.1126/science.207.4433.882

Wang, L. F., Gao, Y. X., Zhang, Y. Z., and Zhang, B. (2012). Research on vertical hydrological cycle of different aquifers in piedmont plain of North China. South North Water Divers. *Water Sci. Technol.* 10 (5), 136–152 [in Chinese with English abstract]. doi:10.3969/j.issn.1672-1683.2012.05.030

Wang, L. F., Liu, J., and Zhao, J. G. (2013). Coseismic slip and post-seismic relaxation of the 2011 M9.0 Tohoku-oki earthquake and its influence on China Mainland. *Earthquake* 33 (4), 238–247. doi:10.3969/j.issn.1000-3274.2013.04.025

Wang, L. F., Liu, J., Zhao, J., and Zhao, J. (2015). Tempo-spatial impact of the 2011 M9 Tohoku-Oki earthquake on eastern China. *Pure Appl. Geophys.* 173 (1), 35–47. doi:10.1007/s00024-015-1121-y

Woith, H. (2015). Radon earthquake precursor: a short review. *Eur. Phys. J. Spec. Top.* 224, 611–627. doi:10.1140/epjst/e2015-02395-9

Xu, S., Zheng, G. D., Wang, X. B., Wang, H., Nakai, S., and Wakita, H. (2014). Helium and carbon isotope variations in Liaodong Peninsula, NE China. *J. Asian Earth Sci.* 90, 149–156. doi:10.1016/j.jseaes.2014.04.019

Yan, R. (2018). Study on the characteristics and mechanism of hydrological changes at Banglazhang hot spring site in Longling county, Yunnan province. Doctoral dissertation. Beijing (China): China university of geosciences [in Chinese with English abstract].

Yang, J. (1997). Hydrochemistry anomaly prior to Wuding M6.5 earthquake. *South China J. Seismol.* 17 (1), 30–37 [in Chinese with English abstract].

Ye, Q., Singh, R. P., He, A., Ji, S., and Liu, C. (2015). Characteristic behavior of water radon associated with Wenchuan and Lushan earthquakes along Longmengshan fault. *Radiat. Meas.* 76, 44–53. doi:10.1016/j.radmeas.2015.04.001

Ye, X., Tao, M., Yu, C., and Zhang, M. (2007). Helium and neon isotopic compositions in the ophiolites from the Yarlung Zangbo River, Southwestern China: the information from deep mantle. *Sci. China Earth Sci.* 50, 801–812. doi:10.1007/s11430-007-0017-9

Zafrir, H. (2008). The evolution, transportation and variation in time of Rn-222 within rocks in a desert 999 region. *Geophys. Res. Abstr.* 10, EGU2008-A-05386.

Zhou, X. C., Liu, L., Chen, Z., Cui, Y. J., and Du, J. G. (2017). Gas geochemistry of the hot spring in the Litang fault zone, Southeast Tibetan Plateau. *Appl. Geochem.* 79, 17–26. doi:10.1016/j.apgeochem.2017.01.022

Zhu, H. G., Li, X. F., and Xu, Y. K. (2020). A helium stratified and ingassed lower mantle: resolving the helium paradoxes. *Acta Geochimica* 39 (1), 4–10. doi:10.1007/s11631-019-00378-2

Zmazek, B., Italiano, F., Zivcic, M., Vaupotič, J., Kobal, I., and Martinelli, G. (2002). Geochemical monitoring of thermal waters in Slovenia: relationships to seismic activity. *Appl. Radiat. Isot.* 57, 919–930. doi:10.1016/s0969-8043(02)00200-2

Conflict of Interest: The authors declare that the research was conducted in the absence of any commercial or financial relationships that could be construed as a potential conflict of interest.

Copyright © 2020 Zhou, Tian, Zhao, Wang and Liu. This is an open-access article distributed under the terms of the Creative Commons Attribution License (CC BY). The use, distribution or reproduction in other forums is permitted, provided the original author(s) and the copyright owner(s) are credited and that the original publication in this journal is cited, in accordance with accepted academic practice. No use, distribution or reproduction is permitted which does not comply with these terms.